

Magnetically Driven and Collimated Jets from the Disc-Magnetosphere Boundary of Rotating Stars

R.V.E. Lovelace, M.M. Romanova, & P. Lii

Department of Astronomy, Cornell University, Ithaca, N.Y. 14853, USA;
RVL1@cornell.edu

E-mail: lovelace@astro.cornell.edu

Abstract. We discuss recent progress in understanding the launching of outflows/jets from the disc-magnetosphere boundary of slowly and rapidly rotating magnetized stars. In most of the discussed models the interior of the disc is assumed to have a turbulent viscosity and magnetic diffusivity (as described by two “alpha” parameters), whereas the coronal region outside of the disc is treated using ideal magnetohydrodynamics (MHD). Extensive MHD simulations have established the occurrence of long-lasting outflows in both the cases of slowly and rapidly rotating stars. (1) In the case of *slowly rotating stars*, a new type of outflow, a *conical wind*, is found and studied in simulations. The conical winds appear in cases where the magnetic flux of the star is bunched up by the inward motion of the accretion disc. Near their region of origin, the winds have the shape of a thin conical shell with a half-opening angle of $\sim 30^\circ$. At large distances these outflows become magnetically collimated by their toroidal magnetic field and form matter dominated jets. That is, the jets are current carrying. About 10–30% of the disc matter flows from the inner disc into the conical winds. The conical winds may be responsible for episodic as well as long-lasting outflows in different types of stars. The predominant driving force for the conical winds is the magnetic force proportional to the negative gradient of the square of the toroidal magnetic field and not the centrifugal force. (2) In the case of *rapidly rotating stars* in the “propeller regime,” a two-component outflow is observed. The first component is similar to the matter dominated conical winds. A large fraction of the disc matter may be ejected into the winds in this regime. The second component is a high-velocity, low-density magnetically dominated *axial jet* where matter flows along the opened polar field lines of the star. The axial jet has a mass flux about 10% that of the conical wind, but its energy flux due to the Poynting flux can be larger than the energy flux of the conical wind. The jet’s angular momentum flux is carried by the magnetic field and causes the star to spin-down rapidly. Such propeller-driven outflows may be responsible for the jets in protostars and for their rapid spin-down.

When the artificial requirement of symmetry about the equatorial plane is dropped, we show that the conical winds may alternately come from one side of the disc and then the other even for the case where the stellar magnetic field is a centered axisymmetric dipole.

Recent MHD simulations of disc accretion to rotating stars in the propeller regime have been done with *no* turbulent viscosity and *no* diffusivity. The strong turbulence we observe is due to the magneto-rotational instability. This turbulence drives accretion in the disc and leads to episodic outflows.

1. Introduction

Outflows in the form of jets and winds are observed from many disc accreting objects ranging from young stars to systems with white dwarfs, neutron stars, and black holes. A large body of observations exists for outflows from young stars at different stages of their evolution, ranging from protostars, where powerful collimated outflows - jets - are observed, to classical T Tauri stars (CTTSs) where the outflows are weaker and often less collimated (see review by Ray et al. 2007). Correlation between the disc's radiated power and the jet power has been found in many CTTSs (Cabrit et al. 1990; Hartigan, Edwards & Gandhour 1995). A significant number of CTTSs show signs of outflows in spectral lines, in particular in He I where two distinct components of outflows had been found (Edwards et al. 2003, 2006; Kwan, Edwards, & Fischer 2007). Outflows are also observed from accreting compact stars such as accreting white dwarfs in symbiotic binaries (Sokoloski & Kenyon 2003), or from the vicinity of neutron stars, such as from Circinus X-1 (Heinz et al. 2007).

Different theoretical models have been proposed to explain the outflows from protostars and CTTSs (see review by Ferreira, Dougados, & Cabrit 2006). The models include those where the outflow originates from a radially distributed disc wind (Blandford & Payne 1982; Königl & Pudritz 2000; Casse & Keppens 2004; Ferreira et al. 2006) or from the innermost region of the accretion disc (Lovelace, Berk & Contopoulos 1991). The latter model is related to the X-wind model (Shu et al. 1994; 2007; Najita & Shu 1994; Cai et al. 2008) where the outflow originates from the vicinity of the disc-magnetosphere boundary. Progress in understanding the theoretical models has come from MHD simulations of accretion discs around rotating magnetized stars as discussed below. Laboratory experiments are also providing insights into jet formation processes (Hsu & Bellan 2002; Lebedev et al. 2005) but these are not discussed here.

Outflows or jets from the disc-magnetosphere boundary were found in early axisymmetric MHD simulations by Hayashi, Shibata & Matsumoto (1996) and Miller & Stone (1997). A one-time episode of outflows from the inner disc and inflation of the innermost field lines connecting the star and the disc were observed for a few dynamical time-scales. Somewhat longer simulation runs were performed by Goodson et al. (1997, 1999), Hirose et al. (1997), Matt et al. (2002) and Küker, Henning & Rüdiger (2003) where several episodes of field inflation and outflows were observed. These simulations hinted at a possible long-term nature for the outflows. However, the simulations were not sufficiently long to establish the behavior of the outflows. MHD simulations showing long-lasting (thousand of orbits of the inner disc) outflows from the disc-magnetosphere have been obtained by our group (Romanova et al. 2009; Lii et al. 2012). We obtained these outflows/jets in two main cases: (1) where the star rotates slowly but the field lines are bunched up into an X-type configuration, and (2) where the star rotates rapidly, in the “propeller regime” (Illarionov & Sunyaev 1975; Alpar & Shaham 1985; Lovelace, Romanova & Bisnovatyi-Kogan 1999). Figure 1 shows the equatorial angular rotation rate $\Omega(r, z = 0)$ of the plasma in the two cases. Here, r_* is the radius of the star;

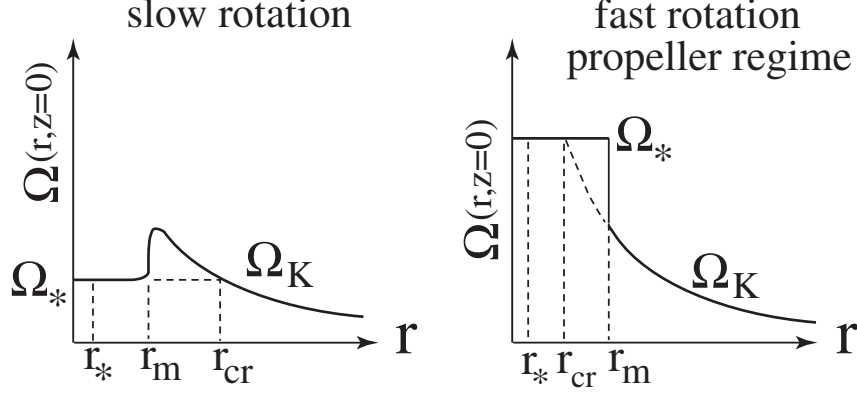


Figure 1. Schematic profiles of the midplane angular velocity of the plasma for the case of a slowly rotating star (left-hand panel) and a rapidly rotating star (right-hand panel) which is in the propeller regime. Here, Ω_* is the angular rotation rate of the star, Ω_K is the Keplerian rotation rate of the disc, r_* is the star’s radius, r_m is the radius of the magnetosphere, and r_{cr} is the co-rotation radius.

r_m is the magnetospheric radius where the kinetic energy density of the disc matter is about equal to the energy density of the magnetic field; and $r_{cr} = (GM/\Omega_*^2)^{1/3}$ is the co-rotation radius where the angular rotation rate of the star Ω_* equals that of the Keplerian disc $\Omega_K = (GM/r^3)^{1/2}$. For a slowly rotating star $r_m < r_{cr}$ whereas for a rapidly rotating star in the propeller regime $r_m > r_{cr}$.

Figure 2 shows examples of the outflows in the two cases. In both cases, two-component outflows are observed: One component originates at the inner edge of the disc near r_m and has a narrow-shell conical shape close to the disc and therefore is termed a “conical wind”. It is matter dominated but can become collimated at large distances due to its toroidal magnetic field. The other component is a magnetically dominated high-velocity “axial jet” which flows along the open stellar magnetic field lines. The axial jet may be very strong in the propeller regime. A detailed discussion of the simulations and analysis can be found in Romanova et al. (2009) and Lii et al. (2012).

Sec. 2 describes the simulations. Sec. 3 discusses the conical winds and axial jets, the driving and collimation forces, and the variability of the winds and jets. Sec. 4 discusses simulation results on one-sided and lop-sided jets. Sec. 5 gives the conclusions.

2. MHD Simulations

We simulate the outflows resulting from disc-magnetosphere interaction using the equations of axisymmetric MHD.

Outside of the disc the flow is described by the equations of ideal MHD. Inside the disc the flow is described by the equations of viscous, resistive MHD. In an inertial

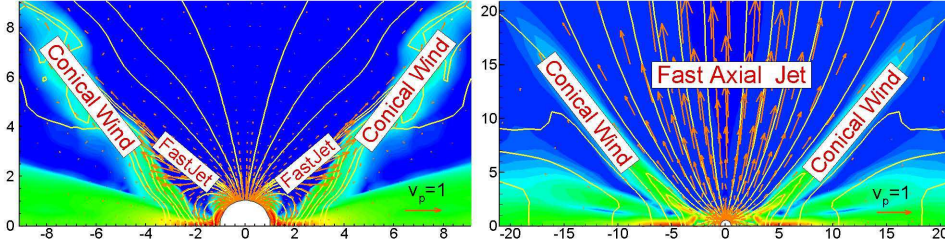


Figure 2. Two-component outflows observed in slowly (left) and rapidly (right) rotating magnetized stars adapted from Romanova et al. (2009). The background shows the poloidal matter flux $F_m = \rho v_p$, the arrows are the poloidal velocity vectors, and the lines are sample magnetic field lines. The labels point to the main outflow components.

reference frame the equations are:

$$\frac{\partial \rho}{\partial t} + \nabla \cdot (\rho \mathbf{v}) = 0, \quad (1)$$

$$\frac{\partial(\rho \mathbf{v})}{\partial t} + \nabla \cdot \mathcal{T} = \rho \mathbf{g}, \quad (2)$$

$$\frac{\partial \mathbf{B}}{\partial t} - \nabla \times (\mathbf{v} \times \mathbf{B}) + \nabla \times (\eta_t \nabla \times \mathbf{B}) = 0, \quad (3)$$

$$\frac{\partial(\rho S)}{\partial t} + \nabla \cdot (\rho S \mathbf{v}) = Q. \quad (4)$$

Here, ρ is the density, S is the specific entropy, \mathbf{v} is the flow velocity, \mathbf{B} is the magnetic field, η_t is the magnetic diffusivity, \mathcal{T} is the momentum flux-density tensor, Q is the rate of change of entropy per unit volume, and $\mathbf{g} = -(GM/r^2)\hat{\mathbf{r}}$ is the gravitational acceleration due to the star, which has mass M . The total mass of the disc is assumed to be negligible compared to M . Here, \mathcal{T} is the sum of the ideal plasma terms *and* the α -viscosity terms discussed in the next paragraph. The plasma is considered to be an ideal gas with adiabatic index $\gamma = 5/3$, and $S = \ln(p/\rho^\gamma)$. We use spherical coordinates (r, θ, ϕ) with θ measured from the symmetry axis. The equations in spherical coordinates are given in Ustyugova et al. (2006).

Both the viscosity and the magnetic diffusivity of the disc plasma are considered to be due to turbulent fluctuations of the velocity and the magnetic field. Both effects are non-zero only inside the disc as determined by a density threshold. The microscopic transport coefficients are replaced by turbulent coefficients. The values of these coefficients are assumed to be given by the α -model of Shakura and Sunyaev (1973), where the coefficient of the turbulent kinematic viscosity is $\nu_t = \alpha_\nu c_s^2 / \Omega_K$, where c_s is the isothermal sound speed and $\Omega_K(r)$ is the Keplerian angular velocity. We take into account the viscous stress terms $\mathcal{T}_{r\phi}^{\text{vis}}$ and $\mathcal{T}_{\theta\phi}^{\text{vis}}$ (Lii et al. 2012). Similarly, the coefficient of the turbulent magnetic diffusivity $\eta_t = \alpha_\eta c_s^2 / \Omega_K$. Here, α_ν and α_η are dimensionless coefficients which are treated as parameters of the model.

Table 1. Reference values for different types of stars. We choose the mass M , radius R_* , equatorial magnetic field B_* and the period P_* of the star and derive the other reference values. The reference mass M_0 is taken to be the mass M of the star. The reference radius is taken to be twice the radius of the star, $R_0 = 2R_*$. The surface magnetic field B_* is different for different types of stars. The reference velocity is $v_0 = (GM/R_0)^{1/2}$. The reference time-scale $t_0 = R_0/v_0$, and the reference angular velocity $\Omega_0 = 1/t_0$. We measure time in units of $P_0 = 2\pi t_0$ (which is the Keplerian rotation period at $r = R_0$). In the plots we use the dimensionless time $T = t/P_0$. The reference magnetic field is $B_0 = B_*(R_*/R_0)^3/\tilde{\mu}$, where $\tilde{\mu}$ is the dimensionless magnetic moment which has a numerical value of 10 in the simulations discussed here. The reference density is taken to be $\rho_0 = B_0^2/v_0^2$. The reference pressure is $p_0 = B_0^2$. The reference temperature is $T_0 = p_0/\mathcal{R}\rho_0 = v_0^2/\mathcal{R}$, where \mathcal{R} is the gas constant. The reference accretion rate is $\dot{M}_0 = \rho_0 v_0 R_0^2$. The reference energy flux is $\dot{E}_0 = \dot{M}_0 v_0^2$. The reference angular momentum flux is $\dot{L}_0 = \dot{M}_0 v_0 R_0$. The poloidal magnetic field of the star (in the absence of external plasma) is an aligned dipole field.

	Protostars	CTTSs	Brown dwarfs	White dwarfs	Neutron stars
$M(M_\odot)$	0.8	0.8	0.056	1	1.4
R_*	$2R_\odot$	$2R_\odot$	$0.1R_\odot$	5000 km	10 km
R_0 (cm)	$2.8 \cdot 10^{11}$	$2.8 \cdot 10^{11}$	$1.4 \cdot 10^{10}$	10^9	$2 \cdot 10^6$
v_0 (cm s $^{-1}$)	$1.95 \cdot 10^7$	$1.95 \cdot 10^7$	$1.6 \cdot 10^7$	$3.6 \cdot 10^8$	$9.7 \cdot 10^9$
P_*	1.04 days	5.6 days	0.13 days	89 s	6.7 ms
P_0	1.04 days	1.04 days	0.05 days	17.2 s	1.3 ms
B_* (G)	$3.0 \cdot 10^3$	10^3	$2 \cdot 10^3$	10^6	10^9
B_0 (G)	37.5	12.5	25.0	$1.2 \cdot 10^4$	$1.2 \cdot 10^7$
ρ_0 (g cm $^{-3}$)	$3.7 \cdot 10^{-12}$	$4.1 \cdot 10^{-13}$	$1.4 \cdot 10^{-12}$	$1.2 \cdot 10^{-9}$	$1.7 \cdot 10^{-6}$
n_0 (cm $^{-3}$)	$2.2 \cdot 10^{12}$	$2.4 \cdot 10^{11}$	$8.5 \cdot 10^{11}$	$7 \cdot 10^{14}$	10^{18}
$\dot{M}_0(M_\odot \text{yr}^{-1})$	$1.8 \cdot 10^{-7}$	$2 \cdot 10^{-8}$	$1.8 \cdot 10^{-10}$	$1.3 \cdot 10^{-8}$	$2 \cdot 10^{-9}$
\dot{E}_0 (erg s $^{-1}$)	$2.1 \cdot 10^{33}$	$2.4 \cdot 10^{32}$	$2.5 \cdot 10^{30}$	$5.7 \cdot 10^{34}$	$6 \cdot 10^{36}$
\dot{L}_0 (erg s $^{-1}$)	$3.1 \cdot 10^{37}$	$3.4 \cdot 10^{36}$	$1.7 \cdot 10^{33}$	$1.6 \cdot 10^{35}$	$1.2 \cdot 10^{33}$
T_d (K)	2290	4590	5270	$1.6 \cdot 10^6$	$1.1 \cdot 10^9$
T_c (K)	$2.3 \cdot 10^6$	$4.6 \cdot 10^6$	$5.3 \cdot 10^6$	$8 \cdot 10^8$	$5.6 \cdot 10^{11}$

The MHD equations are solved in dimensionless form so that the results can be readily applied to different accreting stars.

The system of MHD equations (1-4) have been integrated numerically in spherical (r, θ, ϕ) coordinates using a Godunov-type numerical scheme. The calculations were done in the region $R_{\text{in}} \leq r \leq R_{\text{out}}$, $0 \leq \theta \leq \pi/2$. The grid is uniform in the θ -direction with N_θ cells. The N_r cells in the radial direction have $dr_{j+1} = (1 + 0.0523)dr_j$ ($j = 1..N_r$) so that the poloidal-plane cells are curvilinear rectangles with approximately equal sides. This choice results in high spatial resolution near the star where the disc-magnetosphere interaction takes place while also permitting a large simulation region. We have used a range of resolutions going from $N_r \times N_\theta = 51 \times 31$ to 121×51 .

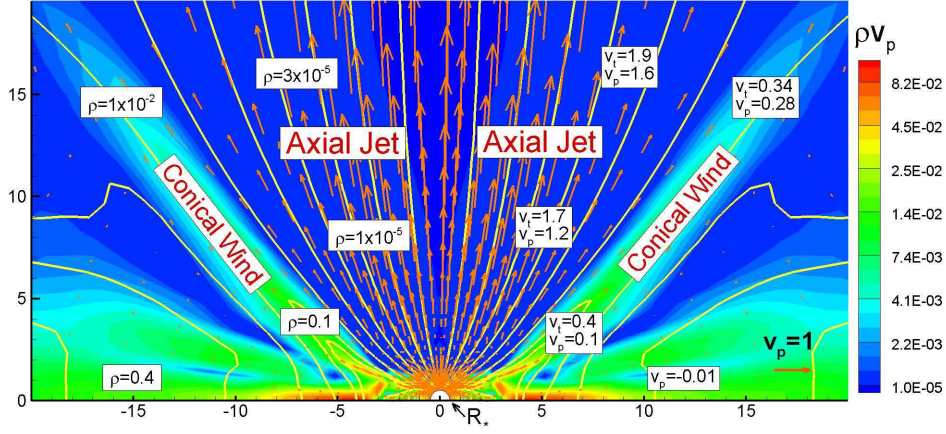


Figure 3. Matter flux ρv_p (background), sample field lines, and poloidal velocity vectors in a propeller-driven outflow at time $t = 1400$ (rotations at $r = 1$) adapted from Romanova et al. (2009). Sample numerical values are given for the poloidal v_p and total v_t velocity, and for the density ρ for different parts of the simulation region. One can see from the Table 1 that for CTTs $v_p = 1$ corresponds to $v_p = 195$ km/s in dimensional units. Unit density corresponds to $\rho_0 = 4.1 \times 10^{-13}$ g cm $^{-3}$. Dimensionless data shown on the plot can be converted to dimensional units for other types of stars using the reference values from the Table 1.

3. Conical Winds and Axial Jets

A large number of simulations were done in order to understand the origin and nature of conical winds. All of the key parameters were varied in order to ensure that there is no special dependence on any parameter. We observed that the formation of conical winds is a common phenomenon for a wide range of parameters. They are most persistent and strong in cases where the viscosity and diffusivity coefficients are not very small, $\alpha_\nu \gtrsim 0.03$, $\alpha_\eta \gtrsim 0.03$. Another important condition is that $\alpha_\nu \gtrsim \alpha_\eta$; that is, the magnetic Prandtl number of the turbulence, $\mathcal{P}_m = \alpha_\nu / \alpha_\eta \gtrsim 1$. This condition favors the bunching of the stellar magnetic field by the accretion flow.

Figure 3 shows a snapshot from our simulations at time $t = 1400$ for the propeller regime. The figure shows the dimensionless density and velocity at sample points. One can see that the velocities in the conical wind component are similar to those in conical winds around slowly rotating stars. Matter launched from the disc initially has an approximately Keplerian azimuthal velocity, $v_K = \sqrt{GM_*/r}$. It is gradually accelerated to poloidal velocities $v_p \sim (0.3 - 0.5)v_K$ and the azimuthal velocity decreases. The flow has a high density and carries most of the disc mass into the outflows. The situation is the opposite in the axial jet component where the density is $10^2 - 10^3$ times lower, while the poloidal and total velocities are significantly higher. Thus we find a *two-component outflow*: a matter dominated conical wind and a magnetically dominated axial jet.

We observe conical winds in both slowly and rapidly rotating stars. In both cases, matter in the conical winds passes through the Alfvén surface (and shortly thereafter through the fast magnetosonic point), beyond which the flow is matter-dominated in

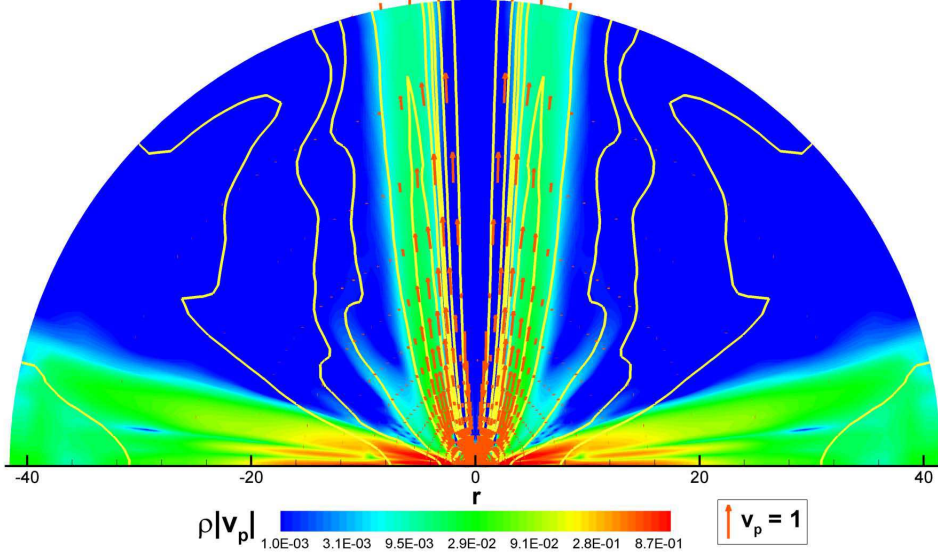


Figure 4. The conical wind/jet from a slowly rotating star at time $t = 860$ adapted from Lii et al. (2012). The background shows the poloidal matter flux density $\rho \mathbf{v}_p$ and the lines show the poloidal projections of the magnetic field. The red vectors show the poloidal matter velocity \mathbf{v}_p . Dimensional values can be obtained from Table 1. For example for a CTTS, $t_0 = 0.366$ days, $R_0 = 2R_\odot$, $t = 860$ corresponds to 315 days, and the simulation region is 0.39 AU in radius. The horizontal axis shows the distance from the star in units of the reference radii R_0 . For this case $\alpha_\nu = 0.3$ and $\alpha_\eta = 0.1$.

the sense that the energy flow is carried mainly by the matter. The situation is different for the axial jet component where the flow is sub-Alfvénic within the simulation region. For this component the energy flow is carried by the Poynting flux and the angular momentum flow is carried by the magnetic field.

Collimation and Driving of the Outflows: Figure 4 shows the long-distance development of a conical wind from a slowly rotating star. At large distances the conical wind becomes collimated.

To understand the collimation we analyzed total force (per unit mass) perpendicular to a poloidal magnetic field line (Lii et al. 2012). For distances beyond the Alfvén surface of the flow this force is approximately

$$f_{\text{tot},\perp} = -v_p^2 \frac{\partial \Theta}{\partial s} - \frac{1}{8\pi\rho} \frac{\partial \mathbf{B}_p^2}{\partial n} - \frac{1}{8\pi\rho(r \sin \theta)^2} \frac{\partial (r \sin \theta B_\phi)^2}{\partial n} + \frac{v_\phi^2 \cos \Theta}{r \sin \theta}. \quad (5)$$

(Ustyugova et al. 1999). Here, Θ is the angle between the poloidal magnetic field and the symmetry axis, s is the arc length along the poloidal field line, n is a coordinate normal to the poloidal field, and the p -subscripts indicate the poloidal component of a vector. Once the jet begins to collimate, the curvature term $-v_p^2 \partial \Theta / \partial s$ also becomes negligible. The magnetic force may act to either collimate or decollimate the jet, depending on the relative magnitudes of the toroidal $(r \sin \theta B_\phi)^2$ gradient (which collimates the outflow) and poloidal \mathbf{B}_p^2 gradient (which “decollimates”). In our simulations, the collimation of the matter implies that the magnetic hoop stress is larger than the poloidal field

gradient. Thus the main perpendicular forces acting in the jet are the collimating effect of the toroidal magnetic field and the decollimating effect of the centrifugal force and the gradient of \mathbf{B}_p^2 . The collimated effect of B_ϕ dominates. Note that in MKS units $2\pi r \sin \theta B_\phi / \mu_0$ is the poloidal current flowing through a surface of radius r from colatitude zero to θ . For the jets from young stars this current is of the order of 2×10^{13} A.

The driving force for the outflow is simply the force parallel to the poloidal magnetic field of the flow $f_{\text{tot},\parallel}$. This is obtained by taking the dot product of the Euler equation with the $\hat{\mathbf{b}}$ unit vector which is parallel to the poloidal magnetic field line \mathbf{B}_p . The derivation by Ustyugova et al. (1999) gives

$$f_{\text{tot},\parallel} = -\frac{1}{\rho} \frac{\partial P}{\partial s} - \frac{\partial \Phi}{\partial s} + \frac{v_\phi^2}{r \sin \theta} \sin \Theta + \frac{1}{4\pi\rho} \hat{\mathbf{b}} \cdot [(\nabla \times \mathbf{B}) \times \mathbf{B}]. \quad (6)$$

Here, the terms on the right-hand side correspond to the pressure, gravitational, centrifugal and magnetic forces, respectively denoted $\mathbf{f}_{\text{p,G,C,M}}$. The pressure gradient force, \mathbf{f}_p , dominates within the disk. The matter in the disk is approximately in Keplerian rotation such that the sum of the gravitational and centrifugal forces roughly cancel ($\mathbf{f}_{\text{G+C}} \approx 0$). Near the slowly rotating star, however, the matter is strongly coupled to the stellar magnetic field and the disk orbits at sub-Keplerian speeds, giving $\mathbf{f}_{\text{G+C}} \lesssim 0$. The magnetic driving force (the last term of Eq. 6) can be expanded as

$$f_{\text{M},\parallel} = -\frac{1}{8\pi\rho(r \sin \theta)^2} \frac{\partial}{\partial s} (r \sin \theta B_\phi)^2, \quad (7)$$

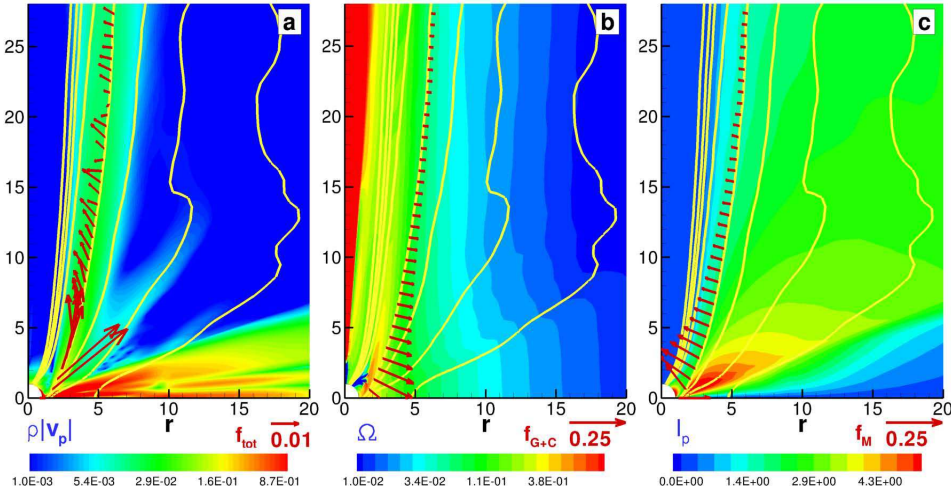


Figure 5. Forces along a field line in the jet adapted from Lii et al. (2012). **Panel (a)** shows the poloidal matter flux density $\rho|\mathbf{v}_p|$ as a background overplotted with poloidal magnetic field lines. The vectors show the *total* force \mathbf{f}_{tot} along a representative field line originating from the disk at $r = 1.24$. **Panel (b)** plots the angular velocity Ω as the background. The vectors show the sum of the *gravitational + centrifugal* forces $\mathbf{f}_{\text{G+C}}$ along the representative field line. **Panel (c)** shows the poloidal current I_p as the background. The vectors show the total *magnetic* force \mathbf{f}_M along the representative field line.

(Lovelace et al. 1991).

Figure 5 shows the variation of the total force \mathbf{f}_{tot} , the gravitational plus centrifugal force, and the magnetic force along a representative field line. This analysis establishes that the predominant driving force for the outflow is the magnetic force (Eq. 7) and not the centrifugal force. This is in agreement with the analysis of Lovelace et al. (1991).

Variability: For both rapidly and slowly rotating stars the magnetic field lines connecting the disc and the star have the tendency to inflate and open (Lovelace, Romanova & Bisnovatyi-Kogan 1995). Quasi-periodic reconstruction of the magnetosphere due to inflation and reconnection has been discussed theoretically (Aly & Kuipers 1990) and has been observed in a number of axisymmetric simulations (Hirose et al. 1997; Goodson et al. 1997, 1999; Matt et al. 2002; Romanova et al. 2002). Goodson & Winglee (1999) discuss the physics of inflation cycles. They have shown that each cycle of inflation consists of a period of matter accumulation near the magnetosphere, diffusion of this matter through the magnetospheric field, inflation of the corresponding field lines, accretion of some matter onto the star, and outflow of some matter as winds, with subsequent expansion of the magnetosphere. Their simulations show 5 – 6 cycles of inflation and reconnection. Our simulations often show 30 – 50 cycles of inflation and reconnection. Figure 6 shows the time evolution of the accretion rates for a slowly rotating star (Romanova et al. 2009).

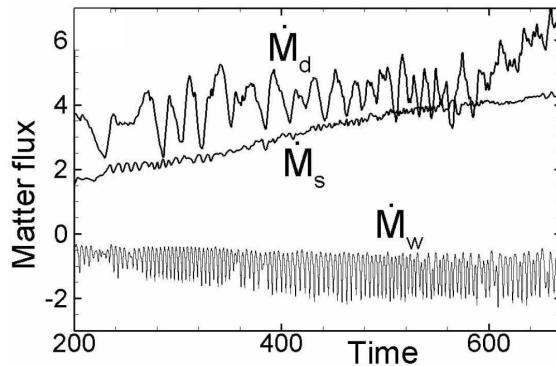


Figure 6. Matter flux onto the star \dot{M}_s , into the conical wind \dot{M}_w , and through the disk \dot{M}_d .

Kurosawa and Romanova (2012) have calculated spectra from modeled conical winds using the radiative transfer code TORUS and have shown that conical winds may explain different features in the hydrogen spectral lines, in the He I line and also a relatively narrow, low-velocity blue-shifted absorption components in the He I $\lambda 10830$ which is often seen in observations (Kurosawa et al. 2011).

4. One-Sided and Lop-Sided Jets

There is clear evidence, mainly from Hubble Space Telescope (HST) observations, of the asymmetry between the approaching and receding jets from a number of young stars.

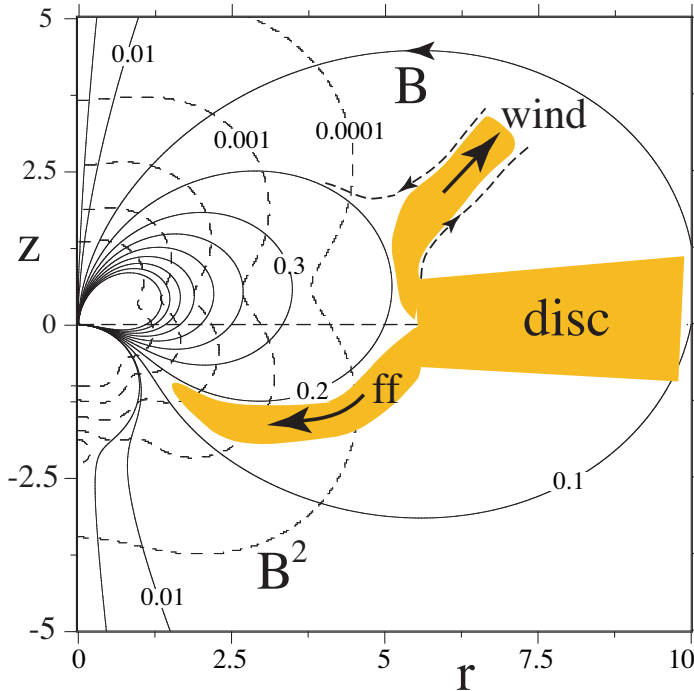


Figure 7. The initial poloidal magnetic field lines and constant magnetic pressure lines for the case of an aligned dipole and quadrupole field adapted from Lovelace et al. (2010). The funnel flow (ff) and the wind in this figure are suggested. The dashed lines are constant values of B^2 .

The objects include the jets in HH 30 (Bacciotti et al. 1999), RW Aur (Woitas et al. 2002), TH 28 (Coffey et al. 2004), and LkH α 233 (Perrin & Graham 2007). Specifically, the radial speed of the approaching jet may differ by a factor of two from that of the receding jet. For example, for RW Aur the radial redshifted speed is ~ 100 km/s whereas the blueshifted radial speed is ~ 175 km/s. The mass and momentum fluxes are also significantly different for the approaching and receding jets in a number of cases. Of course, it is possible that the observed asymmetry of the jets could be due to say differences in the gas densities on the two sides of the source. Here, we discuss the case of intrinsic asymmetry where the asymmetry of outflows is connected with asymmetry of the star's magnetic field. Substantial observational evidence points to the fact that young stars often have *complex* magnetic fields consisting of dipole, quadrupole, and higher order poles misaligned with respect to each other and the rotation axis (Jardine et al. 2002; Donati et al. 2008). Analysis of the plasma flow around stars with realistic fields have shown that a fraction of the star's magnetic field lines are open and may carry outflows (e.g., Gregory et al. 2006).

It is evident that the complex magnetic field of a star will destroy the commonly assumed symmetry of the magnetic field and the plasma about the equatorial plane. Figure 7 shows an illustrative complex magnetic field consisting of the combination of a

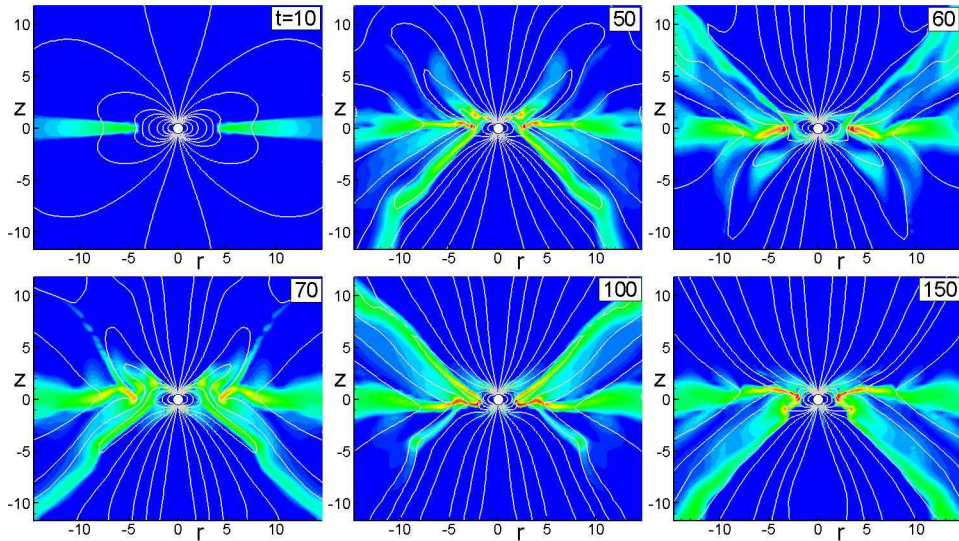


Figure 8. "Flip-flop" of outflows in the case where the stellar magnetic field is a centered axisymmetric dipole adapted from Lovelace et al. (2010). The color background shows the matter flux distribution, and the lines are the poloidal magnetic field lines.

dipole and a quadrupole field both of which are axisymmetric. The figure includes the suggested locations of the funnel flow to the star (Romanova et al. 2002) and the conical wind outflows. The MHD simulations fully support the qualitative picture suggested in Figure 7 (Lovelace et al. 2010). The time-scale during which the jet comes from the upper hemisphere is set by the evolution time-scale for the stellar magnetic field. This is determined by the dynamo processes responsible for the generation of the field.

Remarkably, once the assumption of symmetry about the equatorial plane is dropped, we find that the conical winds alternately come from one hemisphere and then the other *even* when the stellar magnetic field is a centered axisymmetric dipole (Lovelace et al. 2010). An illustrative case of this spontaneous symmetry breaking is shown in Figure 8. The time-scale for the 'flipping' is the accretion time-scale of the inner part of the disc which is expected to be much less than the evolution time of the star's magnetic field.

5. Conclusions

Detailed magnetohydrodynamic simulations have established that long-lasting outflows of cold disc matter into a hot low-density corona from the disc-magnetosphere boundary in cases of slowly and rapidly rotating stars. The main results are the following:

For slowly rotating stars a new type of outflow — a conical wind — has been discovered. Matter flows out forming a *conical wind* which has the shape of a thin conical shell with a half-opening angle $\theta \sim 30^\circ$. The outflows appear in cases where the magnetic flux of the star is bunched up by the inward accretion flow of the disc. We find that this occurs when the turbulent magnetic Prandtl number (the ratio of viscosity to

diffusivity) $\mathcal{P}_m > 1$, and when the viscosity is sufficiently high, $\alpha_\nu \gtrsim 0.03$.

Winds from the disc-magnetosphere boundary have been proposed earlier by Shu and collaborators and referred to as X-winds (Shu et al. 1994). In this model, the wind originates from a small region near the corotation radius r_{cr} , while the disc truncation radius r_t (or, the magnetospheric radius r_m) is only slightly smaller than r_{cr} ($r_m \approx 0.7r_{\text{cr}}$, Shu et al. 1994). It is suggested that excess angular momentum flows from the star to the disc and from there into the X-winds. The model aims to explain the slow rotation of the star and the formation of jets. In the simulations discussed here we have obtained outflows from both slowly and rapidly rotating stars. Both have conical wind components which are reminiscent of X-winds. In some respects the conical winds are similar to X-winds: They both require *bunching* of the poloidal field lines and show outflows from the inner disc; and they both have high rotation and show gradual poloidal acceleration (e.g., Najita & Shu 1994).

The main differences are the following: (1) The conical/propeller outflows have *two components*: a slow high-density conical wind (which can be considered as an analogue of the X-wind), and a fast low-density jet. No jet component is discussed in the X-wind model. (2) Conical winds form around stars with *any rotation rate* including very slowly rotating stars. They do not require fine tuning of the corotation and truncation radii. For example, bunching of field lines is often expected during periods of enhanced or unstable accretion when the disc comes closer to the surface of the star and $r_m \ll r_{\text{cr}}$. Under this condition conical winds will form. In contrast, X-winds require $r_m \approx r_{\text{cr}}$. (3) The base of the conical wind component in both slowly and rapidly rotating stars is associated with the region where the field lines are bunched up, and not with the corotation radius. (4) X-winds are driven by the *centrifugal force*, and as a result matter flows over a wide range of directions below the “dead zone” (Shu et al. 1994; Ostriker & Shu 1995). In conical winds the matter is driven by the *magnetic force* (Lovelace et al. 1991) which acts such that the matter flows into a *thin shell* with a cone half-angle $\theta \sim 30^\circ$. The same force tends to collimate the flow.

For rapidly rotating stars in the propeller regime where $r_m > r_{\text{cr}}$ and where the condition for bunching, $\mathcal{P}_m > 1$, is satisfied we find two distinct outflow components (1) a relatively low-velocity conical wind and (2) a high-velocity axial jet. A significant part of the disc matter and angular momentum flows into the conical winds. At the same time a significant part of the rotational energy of the star flows into the magnetically-dominated axial jet. This regime is particularly relevant to protostars, where the star rotates rapidly and has a high accretion rate. The star spins down rapidly due to the angular momentum flow into the axial jet along the field lines connecting the star and the corona. For typical parameters a protostar spins down in 3×10^5 years. The axial jet is powered by the spin-down of the star rather than by disc accretion. The matter fluxes into both components (wind and jet) strongly oscillate due to events of inflation and reconnection. Most powerful outbursts occur every 1 – 2 months. The interval between outbursts is expected to be longer for smaller diffusivities in the disc. Outbursts are accompanied by higher outflow velocities and stronger self-collimation of

both components. Such outbursts may explain the ejection of knots in some CTTSs every few months.

When the artificial requirement of symmetry about the equatorial plane is dropped, MHD simulations reveal that the conical winds may alternately come from one side of the disc and then the other even for the case where the stellar magnetic field is a centered axisymmetric dipole (Lovelace et al. 2010).

In recent work we have studied the disc accretion to rotating magnetized stars in the propeller regime using a new code with very high resolution in the region of the disc (Lii et al. 2013). In this code *no* turbulent viscosity or diffusivity is incorporated, but instead strong turbulence occurs due to the magneto-rotational instability. This turbulence drives the accretion and it leads to episodic outflows.

The authors thank G. V. Ustyugova and A. V. Koldoba for the development of the codes used in the reported simulations. This research was supported in part by NSF grants AST-1008636 and AST-1211318 and by a NASA ATP grant NNX10AF63G; we thank NASA for use of the NASA High Performance Computing Facilities.

References

- Alpar, M.A., & Shaham, J. 1985, *Nature*, 316, 239
- Aly, J.J., & Kijpers, J. 1990, *A&A*, 227, 473
- Bacciotti, F., Eisloffel, J., & Ray, T.P. 1999, *A&A*, 350, 917
- Bessolaz, N., Zanni, C., Ferreira, J., Keppens, R., Bouvier, J. 2008, *A&A*, 478, 155
- Blandford, R.D., & Payne, D.G. 1982, *MNRAS*, 199, 883
- Cabrit, S., Edwards, S., Strom, S.E., & Strom, K.M. 1990, *ApJ*, 354, 687
- Cai, M.J., Shang, H., Lin, H.-H., & Shu, F.H. 2008, *ApJ*, 672, 489
- Casse, F., & Keppens, R. 2004, *ApJ*, 601, 90
- Coffey, D., Bacciotti, F., Woitas, J., Ray, T.P., & Eisloffel, J. 2004, *ApJ*, 604, 758
- Donati, J.-F., Jardine, M. M., Gregory, S. G., Petit, P., Paletou, F., Bouvier, J., Dougados, C., Mènard, F., Cameron, A. C., Harries, T. J., Hussain, G. A. J., Unruh, Y., Morin, J., Marsden, S. C., Manset, N., Aurière, M., Catala, C., Alecian, E. 2008, *MNRAS*, 386, 1234
- Edwards, S., Fischer, W., Hillenbrand, L., Kwan, J. 2006, *ApJ*, 646, 319
- Edwards, S., Fischer, W., Kwan, J., Hillenbrandt, L., Durpee, A.K. 2003, *ApJ*, 599, L41
- Edwards, S. 2009, *Proceedings of the 15th Cambridge Workshop on Cool Stars, Stellar Systems and the Sun*. AIP Conference Proceedings, Volume 1094, pp. 29-38
- Ferreira, J., Dougados, C., & Cabrit, S. 2006, *A&A*, 453, 785
- Goodson, A.P., & Winglee, R. M., 1999, *ApJ*, 524, 159
- Goodson, A.P., Winglee, R. M., & Böhm, K.-H. 1997, *ApJ*, 489, 199
- Goodson, A.P., Böhm, K.-H., Winglee, R. M. 1999, *ApJ*, 524, 142
- Gregory S. G., Jardine M., Simpson I., & Donati J.-F., 2006, *MNRAS*, 371, 999
- Hartigan, P, Edwards, S., & Gandhour, L. 1995, *ApJ*, 452, 736
- Hayashi, M. R., Shibata, K., & Matsumoto, R. 1996, 468, L37
- Heinz, S., Schulz, N. S., Brandt, W. N., & Galloway, D. K. 2007, *ApJ*, 663, L93
- Hirose, S., Uchida, Yu., Shibata, K., & Matsumoto, R. 1997, *PASJ*, 49, 193
- Hsu, S.C. & Bellan, P.M. 2002, *MNRAS*, 334, 257
- Illarionov, A.F., & Sunyaev, R.A. 1975, *A&A*, 39, 185
- Jardine, M., Collier Cameron, A., & Donati, J.-F. 2002, *MNRAS*, 333, 339
- Königl, A., & Pudritz, R. E. 2000, in *Protostars and Planets IV*, Mannings, V., Boss, A.P., Russell, S. S. (eds.), University of Arizona Press, Tucson, p. 759

- Küker, M., Henning, T., & Rüdiger, G. 2003, *ApJ*, 589, 397
- Kurosawa, R., Romanova, M. M., & Harries, T. 2011, *MNRAS*, 416, 2623
- Kurosawa, R., & Romanova, M. M. 2012, *MNRAS*, 426, 2901
- Kwan, J., Edwards, S., & Fischer, W. 2007, *ApJ*, 657, 897
- Lebedev, S. V., Ciardi, A., Ampleford, D. J., Bland, S. N., Bott, S. C., Chittenden, J. P., Hall, G. N., Rapley, J., Jennings, C. A., Frank, A., Blackman, E. G., & Lery, T. 2005, *MNRAS*, 361, 97
- Lii, P.S., Romanova, M., & Lovelace, R. 2012, *MNRAS*, 420, 2020
- Lii, P.S., Romanova, M.M., Ustyugova, G.V., Koldoba, A.V., & Lovelace, R.V.E. 2013, *MNRAS*, in press (arXiv: 1304.2703v1)
- Lovelace, R.V.E., Berk, H.L., & Contopoulos, J. 1991, *ApJ*, 379, 696
- Lovelace, R.V.E., Romanova, M.M., & Bisnovatyi-Kogan, G.S. 1995, *MNRAS*, 275, 244
- Lovelace, R.V.E., Romanova, M.M., & Bisnovatyi-Kogan, G.S. 1999, *ApJ*, 514, 368
- Lovelace, R. V. E., Romanova, M. M., Ustyugova, G. V., & Koldoba, A. V. 2010, *MNRAS*, 408, 2083
- Matt, S., Goodson, A.P., Winglee, R.M., & Böhm, K.-H. 2002, *ApJ*, 574, 232
- Miller, K.A., & Stone, J.M. 1997, *ApJ*, 489, 890
- Najita, J.R., & Shu, F.H. 1994, *ApJ*, 429, 808
- Ostriker, E.C., & Shu, F.H. 1995, *ApJ*, 447, 813
- Perrin, M.D., & Graham, J.R. 2007, *ApJ*, 670, 499
- Romanova, M.M., Ustyugova, G.V., Koldoba, A.V., & Lovelace, R.V.E. 2002, *ApJ*, 578, 420
- Romanova, M.M., Ustyugova, G.V., Koldoba, A.V., & Lovelace, R.V.E. 2009, *MNRAS*, 399, 1802
- Shakura, N.I., & Sunyaev, R.A. 1973, *A&A*, 24, 337
- Shu, F., Najita, J., Ostriker, E., Wilkin, F., Ruden, S., Lizano, S. 1994, *ApJ*, 429, 781
- Shu, F.H., Galli, D., Lizano, S., Glassgold, A.E., & Diamond, P.H. 2007, *ApJ*, 665, 535
- Sokoloski, J.L., & Kenyon, S.J. 2003, *ApJ*, 584, 1021
- Ustyugova, G.V., Koldoba, A.V., Romanova, M.M., Chechetkin, V.M., & Lovelace, R.V.E. 1999, *ApJ*, 516, 221
- Ustyugova, G.V., Koldoba, A.V., Romanova, M.M., & Lovelace, R.V.E. 2006, *ApJ*, 646, 304
- Woitats, J., Ray, T.P., Bacciotti, F., Davis, C.J., & Eisloffel, J. 2002, *ApJ*, 580, 336